Hindawi
Journal of Nanomaterials
Volume 2019, Article ID 6532967, 8 pages
https://doi.org/10.1155/2019/6532967

Research Article

Far-Field Analysis on Reflecting Colors of Dielectric Nanosphere Metasurface

Seokhyeon Hong, Young Jin Lee, Kihwan Moon, Youngsoo Kim, Eunso Shin, and Soon-Hong Kwon

Department of Physics, Chung-Ang University, Seoul 06974, Republic of Korea

Correspondence should be addressed to Soon-Hong Kwon; shkwon@cau.ac.kr

Received 24 November 2018; Revised 29 April 2019; Accepted 19 May 2019; Published 16 June 2019

Academic Editor: Alexey P. Popov

Photonic resonances in nanostructures have been exploited in reflective or transmission color filters, which can provide vivid colors. Metallic nanostructures have been widely studied to demonstrate a variety of color filters based on strong light interaction due to plasmonic resonances. However, because of the severe absorption loss of metal in visible light, dielectric nanoparticles having Mie resonances are a popular study focus in recent years to achieve vivid colors. In contrast to the behaviors of point-like electric dipole in metallic nanoparticle, the interplay of the electric and magnetic Mie resonances in dielectric nanoparticle enables a large degree of freedom in manipulating the directivity of light scattering, reflecting/transmitting color, and spontaneous emission rates. Here, we propose a color reflector based on an array of silicon nanoparticles that shows reflectance greater than 70% and vivid colors over the entire visible spectrum range, which covers sRGB color area. Viewing angle dependencies of the color and brightness are also investigated by calculating color-resolved far-field patterns, while exhibiting maintenance of the color and high reflectance over a broad viewing angle.

1. Introduction

Structural color is observed from strong resonant interactions between light and nanostructure to build reflection or scattering of certain colors. In nature, complex nanostructures show iridescent colors in a number of living things such as the Morpho butterfly [1, 2], peacock [3], and sea mouse [4]. Structure color printing can replace pigment/dye-based traditional color printing, because of its vivid and bright colors. In addition, structure colors have advantages in terms of resolution [5], chromaticity [6], and chemical stability [7]. Therefore, engineering of structural colors in photonic nanostructures has recently been one of the several hot topics in nanophotonics. Many types of structural color pixels have been demonstrated based on metallic and dielectric nanostructures, transmission color filters used in image sensors and display devices [8–12], reflective color pixels for patterning images with fine resolution [13–15], and angle-dependent diffractive colors [16, 17].

In general, a structural color has strong color and brightness dependencies on viewing angle, because the color is generated by resonance of light within the nanostructure, as shown in Morpho butterfly [1, 2] or angle-dependent diffractive gratings [16, 17]. Therefore, the strong viewing angle dependencies can be one of the multiple severe obstacles to realize practical color devices in spite of vivid colors of structural color printings.

Because of the strong light interaction with structures due to plasmonic resonances, collective oscillations of free electrons in nanoscale volume of metal, metallic nanostructures have been widely studied for color applications [5–17]. However, inherent metallic absorption loss may hinder the control and broaden the linewidth of resonance in the visible regime, thus limiting applications to a small color gamut and reducing the color brightness.

On the contrary, dielectric nanoparticles, which exhibit Mie resonances in subwavelength particles, have been intensively researched because of their low optical loss and larger

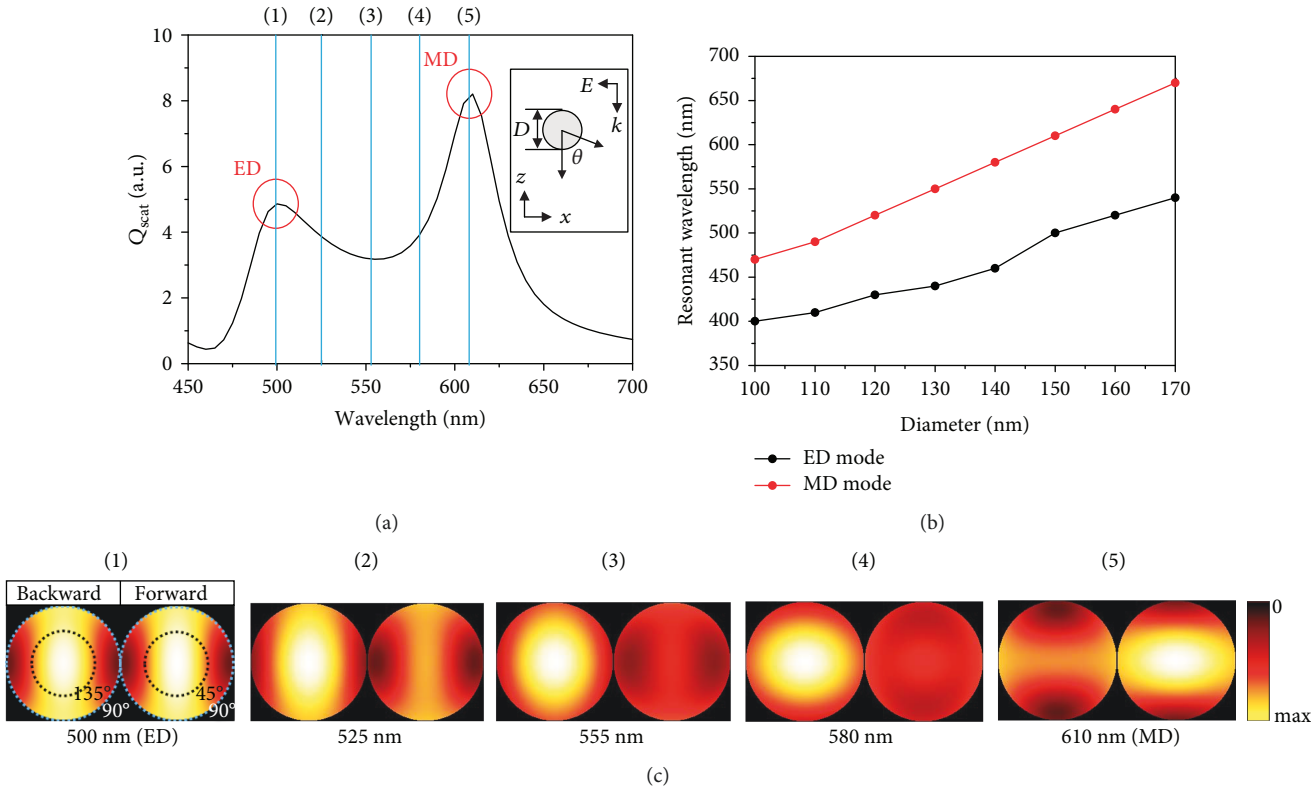

FIGURE 1: (a) Normalized scattering cross section (Q_{scat}) of a silicon nanosphere with a diameter (D) of 150 nm. The inset depicts light scattering by the particle for the incident light along the (-) z direction with E_x linear polarization. The angle θ defines the scattering direction. (b) Resonant wavelengths of electric dipole (ED) and magnetic dipole (MD) modes as functions of Si particle diameter. (c) The far-field patterns of the scattered lights from a Si particle ($D = 150$ nm) for different wavelengths, 500 nm, 525 nm, 555 nm, 580 nm, and 610 nm, indicated by (1), (2), (3), (4), and (5), respectively. In each far-field pattern, the left (right) one presents a backward (forward) scattered light pattern. The dotted line circle denotes 45° for backward/forward directions.

degree of freedoms in designing structures. Specifically, high refractive index subwavelength nanoparticles, such as silicon particles, exhibit clear electric and magnetic Mie resonances in the visible range. Because the interplay between electric and magnetic resonances can manipulate light scattering properties according to the wavelength of incident light, careful design of all dielectric nanoparticles can adjust the scattering of light [18, 19], tailor directional emission [20–22], provide efficient light trapping in photovoltaic devices [23, 24], and generate vivid color [25–27].

A subwavelength-sized dielectric particles show fundamental electric dipole (ED), magnetic dipole (MD), and Mie resonances [22, 28, 29]. The resonant wavelengths of ED and MD modes can be tuned by controlling the size and shape of nanoparticles. Specifically, interactions between two resonant modes have strong backscattering due to the coupling of ED and MD.

Based on the scattering properties of a single dielectric nanoparticle, we propose a color reflector based on an array of the Si nanoparticles on a glass substrate, which shows a variable color spectrum over the entire visible spectrum range covering the sRGB area, while a high reflectance larger than 70% is maintained. In addition, we first calculated color-resolved far-field patterns by obtaining a reflectance spectrum for each viewing angle. The proposed structure can maintain the reflected color for a large range of viewing angles and a high reflectance within a ±40° viewing angle. In contrast to strong angle dependencies of general structure colors in photonic crystals [1, 2] and angle-dependent diffractive gratings [16, 17], the proposed structure exhibits high reflectivity and constant colors over a wide angle due to the large scattering angles of dipole resonances in a single nanosphere. Although transmitted/reflected colors resulted from Mie scatterings of nanoparticles have been widely studied, there are a few of reports on the color and brightness dependencies on the viewing angle. In particular, in our knowledge, the color-resolved far-field pattern analysis on dielectric nanoparticles are firstly reported in this paper. The color-resolved far-field pattern analysis will be useful to design color pixels based on structure colors from nanostructure by providing angular and spectral information of light scattering simultaneously.

2. Results and Discussion

2.1. Scattering of Single Particle. In order to understand light scattering properties from a dielectric nanoparticle, we investigated the normalized scattering cross section (Q_{scat}) of a silicon (Si) nanosphere with a diameter (D) of 150 nm, as shown in Figure 1(a). Here, Q_{scat} is defined by the ratio between the scattering cross section and the geometrical cross section. When an E_x linearly polarized light hits

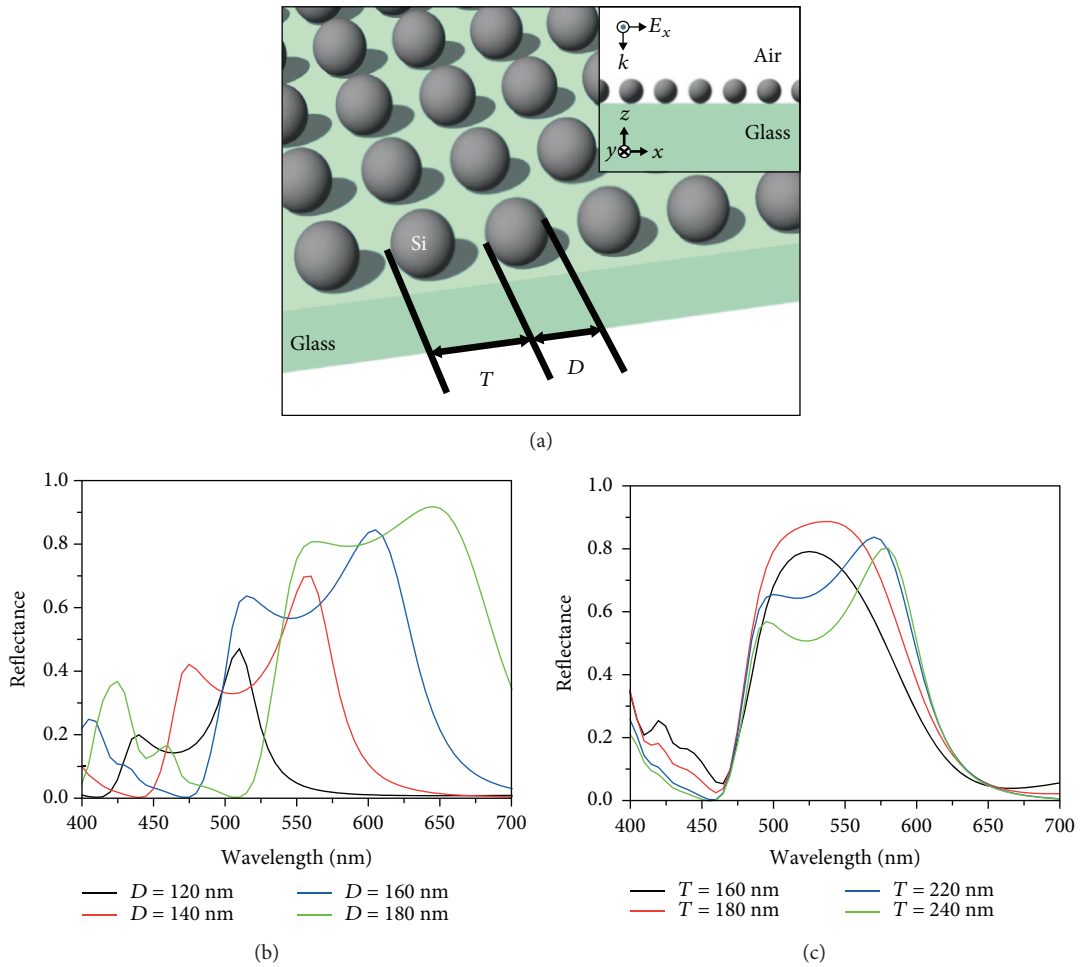

FIGURE 2: (a) Schematic of Si particle array on glass with diameter (D) and period (T). The inset depicts light scattering by the particle array on glass for the incident light along the (-) z direction with E_x linear polarization. Reflectance spectrum of Si particles structures as functions of (b) period (T) and (c) diameter (D) of a Si particle array.

the Si particle, two strong Mie resonant scattering modes, electric dipole (ED) and magnetic dipole (MD) modes, are observed at 500 nm and 610 nm, respectively. Between ED and MD modes (500 nm–610 nm), relatively large scatterings ($Q_{scat} > 3$) are observed. Here, optical properties were simulated by using three-dimensional (3D) finite-difference time-domain (FDTD) method. On the other hand, the resonant wavelengths of ED and MD modes increase as functions of Si nanosphere diameter. As diameter increases from 100 nm to 170 nm, ED (MD) mode redshifts from 400 nm (475 nm) to 525 nm (660 nm) (Figure 1(b)). Therefore, the strong scattering spectral region between ED and MD mode can cover the entire visible spectrum by changing the Si sphere diameter.

In order to investigate the scattering direction, we investigated far-field patterns of scattered light from the Si nanoparticle ($D = 150$ nm) at different wavelengths, 500 nm, 525 nm, 555 nm, 580, and 610 nm (Figure 1(c)), which corresponds to the strong scattering spectral region from ED mode to MD mode. The far-field patterns indicated by (1), (2), (3), (4), and (5), correspond to the spectral position in Figure 1(a). At 500 nm in the ED mode, backward and forward scatterings were similar [18]. At 610 nm in the MD mode, forward scattering was dominant. However, considering incident light with wavelengths between ED and MD modes (525 nm, 555 nm, and 580 nm), strong backward scattering is observed due to the coupling of ED and MD modes [18, 22]. Therefore, a Si nanoparticle shows strong backward scattering for the spectral region between ED and MD modes, as shown in Figures 1(a) and 1(c), and the region can be tuned over the entire visible spectral range.

2.2. Reflected Colors from Silicon Particle Array. Based on the strong backward scattering of a Si nanosphere, we propose a color reflector consisting of a square lattice array of Si nanospheres on a glass substrate, as shown in Figure 2(a), which can exhibit full visible colors with a high reflectance. First, we calculated the reflectance spectrum for different diameters of Si particles, $D = 120$ nm (black), 140 nm (red), 160 nm (blue), and 180 nm (green), respectively, while the period (T) is fixed to 250 nm in Figure 2(b). As diameter increases, the reflectance curve redshifts, as shown by the single particle in Figure 1(b), because the high reflectance originates from the strong backward scatterings between ED and MD modes.

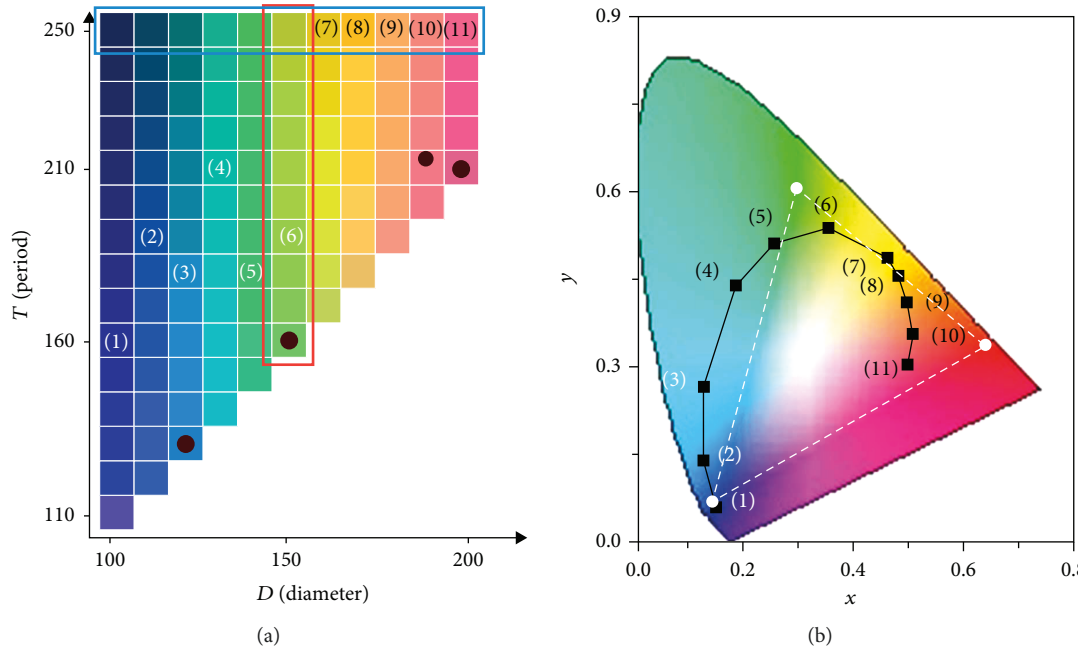

FIGURE 3: (a) Color table of reflectance in an array of silicon for different diameters and periods. (b) Reflected colors of the proposed structure in CIE color coordinates. The sRGB region is represented by white dotted line.

In addition, the reflectance becomes higher with increasing D due to a larger filing factor, defined by the ratio between the area covered by Si particles and the total area.

Next, we investigated the reflectance spectra for different periods, $T = 160$ nm (black), 180 nm (red), 220 nm (blue), and 240 nm (green) with a fixed particle diameter of 160 nm, as shown in Figure 2(c). As period increases, the reflectance became slightly smaller; however, the spectral position of the reflectance curve is nearly maintained. This observation means that the spectral property of the reflectance in an array of Si nanoparticles is manly originated from the scattering property of single nanoparticles. Interactions between particles modify the shape of reflectance curves slightly [27, 30]. When the interaction between nanoparticles becomes weaker at a large period, for example, $T = 240$ nm (green), the reflectance curve is similar to the behavior of the scattering cross section of a single Si particle in Figure 1(a).

We calculated 2D mapping for different diameters and periods of the silicon particle array from the reflectance curves using CIE transformation code, as shown in Figure 3(a). We used a MATLAB code that was adapted from the ciegui package written by Prashant Patil, available on Mathworks File Exchange. Here, the reflectance was calculated by assuming normal incident light with a D65 spectrum.

As particle diameter increased from 100 nm to 200 nm, the color changes from blue to red over the entire visible spectrum range while the period is fixed at 250 nm. In contrast, as shown at the vertical line of $D = 150$ nm, the color is nearly maintained while changing the period. The chromaticity changes only slightly. Figure 3(b) shows the reflected colors in CIE color space. The dots indicated by the numbers of (1), (2),…, (11) represent the outermost colors from the structure, in which the corresponding structure parameters, the diameter, and the period are shown in Figure 3(b). The color area covers a larger color space than the standard sRGB colors indicated by the white dotted line; therefore, the proposed structure can be exploited as a vivid color display.

2.3. Colors of Silicon Particle Array for Different Viewing Angles. On the other hand, the color device needs to maintain the color over wide viewing angles, while covering a large color space. Therefore, we investigated the far field of scattering light from the proposed structure as functions of viewing angle (θ, φ) coordinate, as shown in Figure 4(a). In order to assume the real light environment, we used the standard CIE light source with a D65 spectrum plotted in Figure 4(b), which is not a flat white light source.

In order to check the effect, the color and brightness of the scattered light were investigated for three representative structures with colors of red ($T = 210$ nm, $D = 200$ nm), green ($T = 160$ nm, 150 nm), and blue ($T = 130$ nm, $D = 120$ nm). The representative three structures of Figure 4 are chosen to have the largest RGB area in CIE color coordinate by changing both structure parameters of the period and diameter. Colors of the structures at a normal angle correspond to the colors at the black dots in Figure 3(a). The reflectance of the three investigated structures is shown in Figure 4(c). The peak wavelengths were 475 nm, 530 nm, and 645 nm with a high reflectance larger than 0.7.

In order to investigate the color and brightness on the viewing angle in the scattered lights from the proposed structure, we calculated color-resolved far-field patterns of the three representative RGB structures under a D65 standard light source with normal incidence, as shown in Figure 5(a). To obtain the color-resolved far-field pattern, first, a monochromatic light with a certain wavelength in the visible range from 400 nm to 700 nm was placed normally

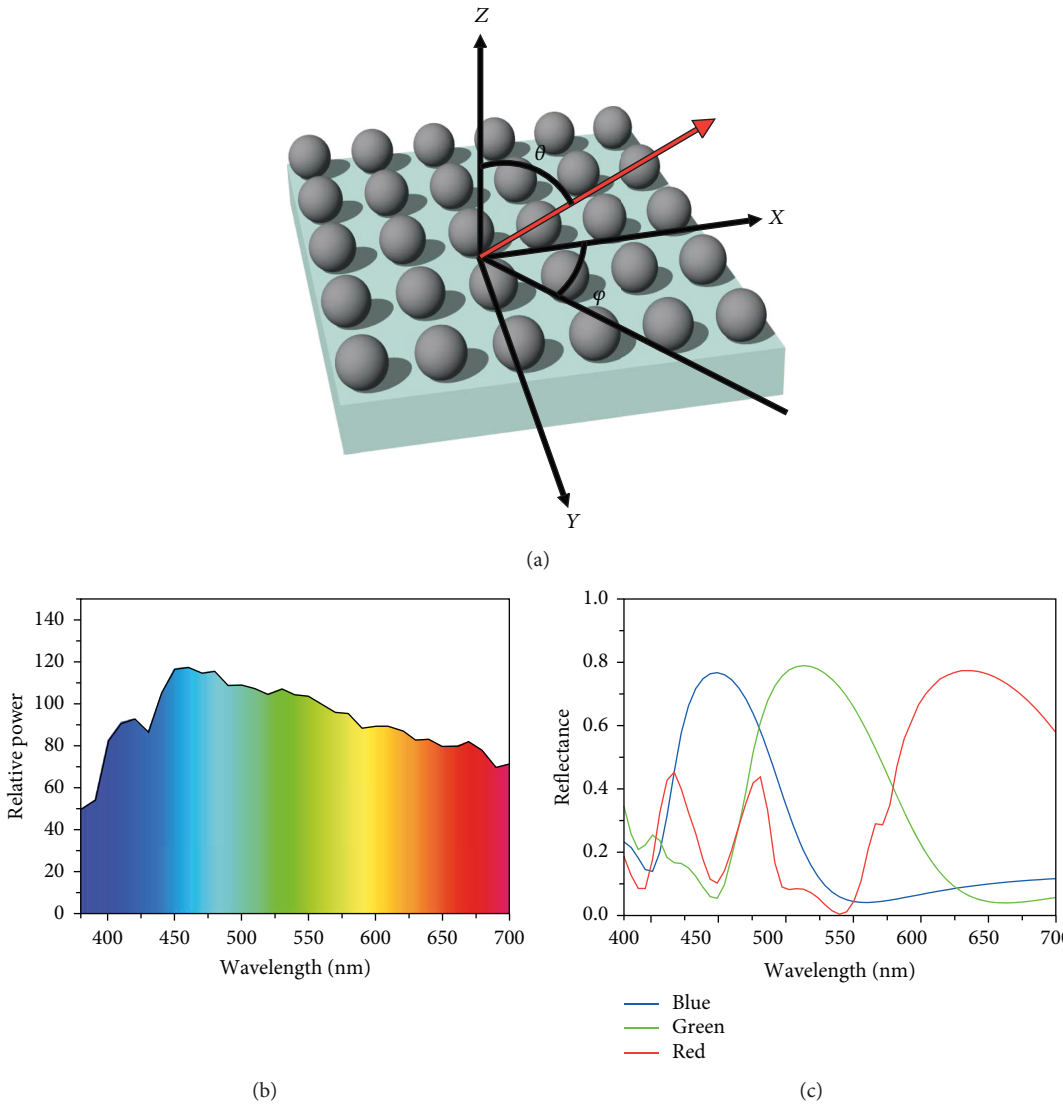

FIGURE 4: (a) Schematic of the coordinate (θ, φ) of the reflected far-field light. Red arrow indicates the scattered light. (b) Reflectance curves of the representative structures for the colors of red ($T = 210$ nm, $D = 200$ nm), green ($T = 160$ nm, 150 nm), and blue ($T = 130$ nm, $D = 120$ nm). The corresponding colors of the structures are shown in black dots of Figure 3(a).

incident on the structure and the monochromatic scattered far field is calculated for the wavelength in a (θ, φ) coordinate. When all monochromatic far-field patterns are calculated for the visible range, the reflectance spectra for each (θ, φ) point, viewing angle, can be obtained while the D65 spectrum is considered. Moreover, the spectrum is converted into the corresponding color of the scattered light for the angle point (θ, φ) by CIE transform. By placing the colors at each angle point, the color-resolved far-field pattern is obtained for the structure, which provides the color and relative brightness for each viewing angle.

In the structure ($T = 160$ nm, $D = 150$ nm) with green color at a normal angle, green color is maintained over the entire viewing angle with negligible color change in the center of Figure 5(a). As the viewing angle increases, the color brightness decreases. All three RGB structures show similar color-resolved far-field patterns, where the representative colors are maintained over the viewing angle with a brightness decrease upon increasing angle. In the angle-resolved scattered light spectrum of Figure 5(b), the reflectance curve shape is maintained for different viewing angles. However, the peak intensity at 525 nm decreases from 0.8 to 0.1 with increasing angle from $\theta = 0^\circ$ (normal reflection) to $\theta = 80^\circ$, yet the color of the scattered lights is maintained for different viewing angles. It should be noted that peak reflectance is 80% and a high reflectance greater than 46% is still achieved for a large viewing angle of 40°. These angular dependencies of the color far-field pattern in the structure with green color are typical for the proposed structure, similar to structures with different colors.

In order to investigate the far-field patterns for different wavelengths, we compared four monochromatic far-field patterns of the structure with green color with wavelengths of 500 nm, 525 nm, 550 nm, and 575 nm in Figure 5(c), which correspond to the high reflectance region of Figure 5(b). All monochromatic far-field patterns were normalized by the

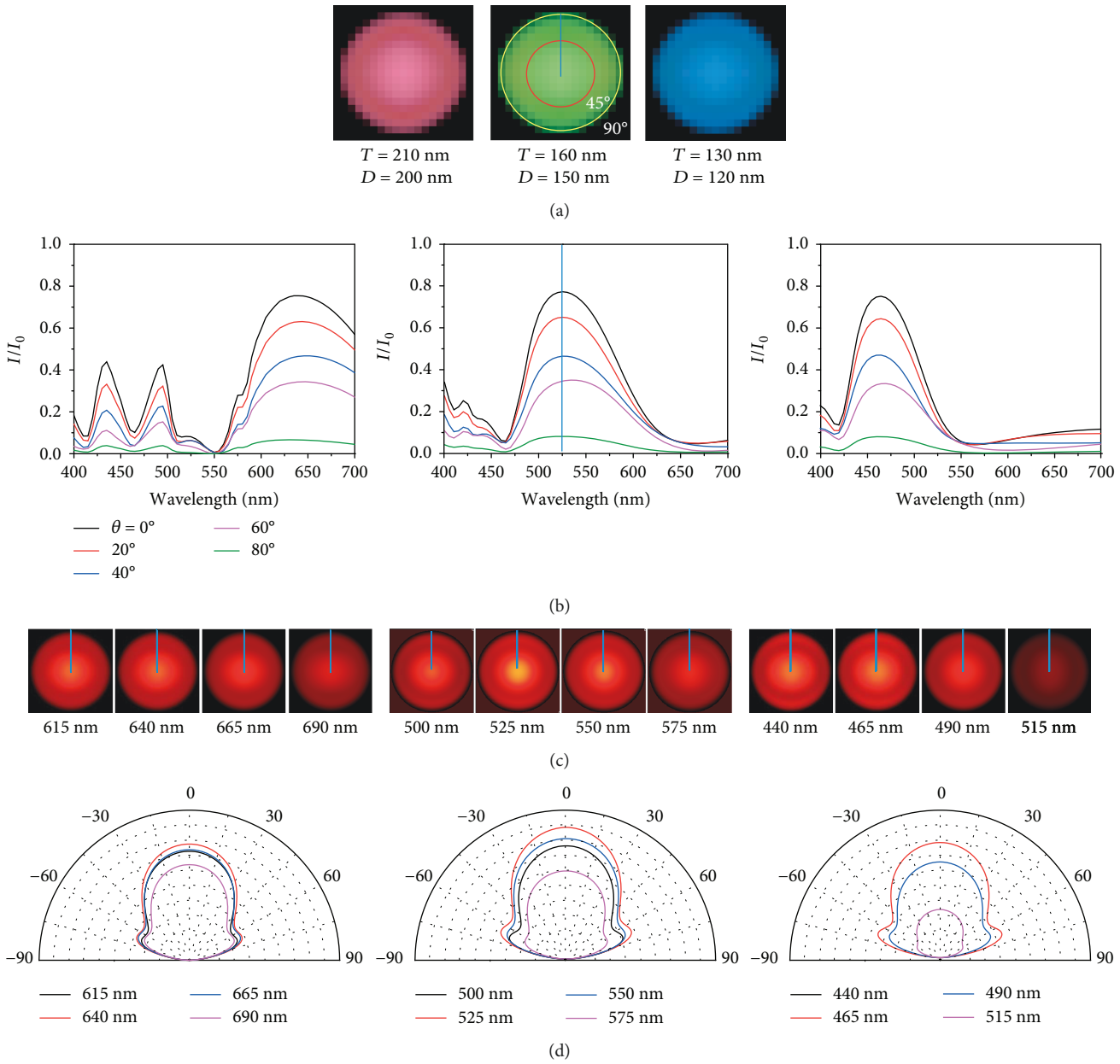

Figure 5: (a) Color-resolved far-field patterns of the three RGB structures in Figure 4(c). The red (yellow) line indicates $\theta = 45^\circ$ (90°). (b) The angle-resolved scattered light spectrum of the red (left), green (center), and blue (right) structures for different viewing angles (θ), 0°, 20°, 40°, 60°, and 80°, which are estimated on the blue dotted line in (a). (c) Scattering monochromatic far-field patterns in the structure with red, green, and blue colors for different wavelengths. All monochromatic patterns are normalized by the maximum far-field value for the peak wavelengths. (d) Scattered far-field intensity as a function of azimuthal angle (θ) at a fixed $\varphi = 0$ for different wavelengths. Red, green, and blue structures are described by ($T = 210$ nm, $D = 200$ nm), ($T = 160$ nm, $D = 150$ nm), and ($T = 130$ nm, $D = 120$ nm).

maximum value of the far field of 525 nm light, e.g., the peak wavelength of the reflectance spectra. As expected in Figure 5(b), the strongest scattered light is observed at 525 nm. In addition, the scattered light distributions over the viewing angle are almost identical for the scattered light at four wavelengths, which proves the color maintenance of the color far-field patterns of Figure 5(a). In the scattered far-field intensity as a function of azimuthal angle (θ) at a fixed $\varphi = 0$ of Figure 5(d), the far-field intensity polar graph is maintained for different wavelengths, 500 nm, 525 nm, 550 nm, and 575 nm, except for the intensity. As mentioned in the case of the green color structure, the red and blue structures also show that high peak reflectance at peak wavelengths is 76% and 75% and, even at a wide viewing angle of 40 degrees, large reflectance of 46% is also guaranteed, as shown in Figures 5(b)–5(d).

Since the far-field pattern of the scattered light is mainly originated from the scattering property of a single silicon nanosphere, the color maintenance over a large viewing angle and the large reflectance over 0.8 are observed in the

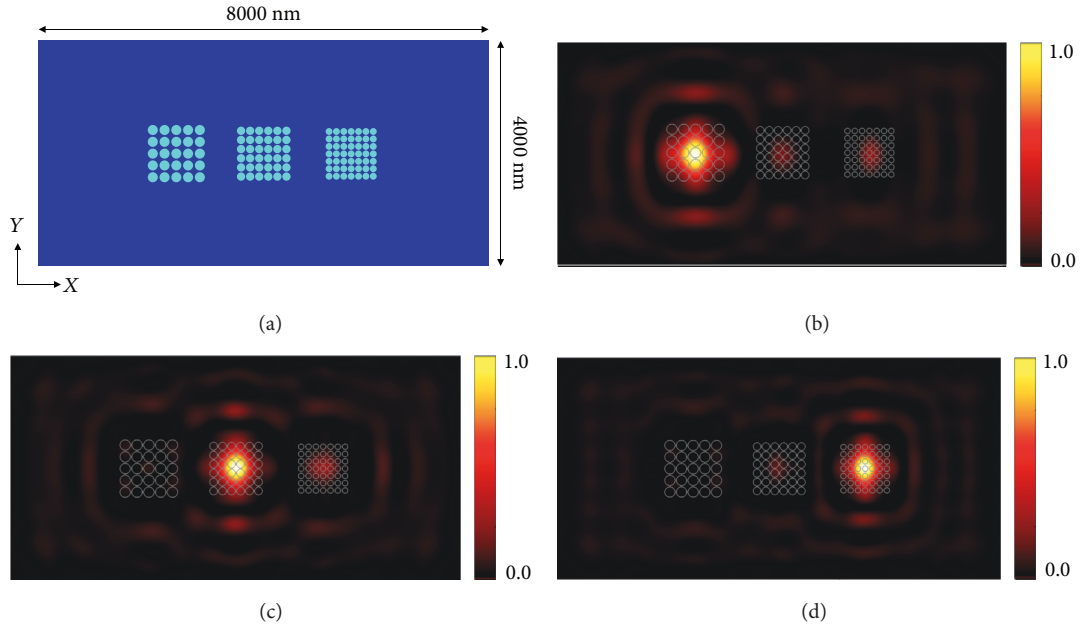

Figure 6: (a) Simple example of an image with three pixels, red, green, and blue pixels. From (a) to (d), red, green, and blue pixels consist of square arrays of silicon nanospheres, described by ($T = 210$ nm, $D = 200$ nm), ($T = 160$ nm, $D = 150$ nm), and ($T = 130$ nm, $D = 120$ nm), respectively. Red, green, and blue arrays are sized by 5×5, 6×6, and 7×7 nanospheres, respectively. Pixels are separated with a distance of 525 nm. Poynting vector images of the reflected light for different incident wavelengths of (b) 640 nm, (c) 525 nm, and (d) 465 nm, which are the peak wavelengths of the reflectance curves of red, green, and blue structures.

wavelength range between ED and MD modes for the proposed structure. In addition, the color-resolved far-field patterns have spherical symmetry, because of the spherical shape of the Si nanoparticle.

In order to show an image with RGB pixels that provide the wide viewing and high reflectance, we suggested simple example consisting of three pixels, red, green and blue pixels, as shown in Figure 6(a). Each pixel consists of square array of silicon nanospheres, corresponding red, green, and blue structures. When normal incident light is reflected and the wavelength is 640 nm, 525 nm, or 465 nm, the peak wavelengths of the reflectance curves of red, green, and blue structures, the reflected light images are calculated by obtaining time averaged, vertically outward Poynting vector images (Figures 6(b)–6(d)). The Poynting vector is measured at the 600 nm above the sphere surface. The reflected light intensity is normalized by assuming the incident light intensity as 1.0. Green light with a wavelength of 525 nm is reflected mostly at the green structure (center structure) with high reflectance (Figure 5(c)). In addition, the reflected light is strongly collimated inside the area of the green structure. Such high reflectance and collimation are also observed in red and blue structures for the light with wavelengths of 640 nm and 465 nm (Figures 5(b) and 5(d)). It means that the suggested image with RGB pixels can show a spatially resolved RGB pixel image even at the wide viewing angle although the separation of 525 nm between the pixels are less than a wavelength.

3. Conclusions

We suggest a dielectric full color reflector consisting of an array of silicon nanospheres on a glass substrate. A silicon nanosphere has two resonances in the visible range due to the electric dipole and magnetic dipole modes, and the coupling between ED and MD induces strong backscattering of the light with a wavelength between the two modes, called the high reflectance region. The proposed structure shows a reflectance greater than 70% due to the strong backscattering. By adjusting the diameter and the period of the silicon particle array, the high reflectance region can cover the entire visible spectral range, which covers most of the sRGB region. Moreover, we investigated the color and brightness of the proposed structures depending on the viewing angle by calculating the far field of the scattering light. As viewing angle increases, the brightness decreases, while the reflectance is still larger than 46% at 40°. The colors are nearly maintained over the entire viewing angle. The proposed structure, which has bright and vivid reflecting colors, can be exploited to develop a reflective-type display. In addition, the color and brightness tolerance over a large viewing angle would be an advantage in a reflective display. The proposed structure can be fabricated by laser printing technique which enables precise deposition of silicon nanospheres [31]. The nanospheres are fixed to the substrate by Van der Waals force [32].

Data Availability

The data used to support the findings of this study are available from the corresponding author upon request.

Conflicts of Interest

No potential conflict of interest was reported by the authors.

Acknowledgments

This work was supported by the National Research Foundation of Korea through the Korean Government under Grant NRF-2019R1A2C4069587.

References

[1] P. Vukusic and J. R. Sambles, "Photonic structures in biology," *Nature*, vol. 424, no. 6950, pp. 852–855, 2003.

[2] Y.-F. Huang, S. Chattopadhyay, Y.-J. Jen et al., "Improved broadband and quasi-omnidirectional anti-reflection properties with biomimetic silicon nanostructures," *Nature Nanotechnology*, vol. 2, no. 12, pp. 770–774, 2007.

[3] J. Zi, X. Yu, Y. Li et al., "Coloration strategies in peacock feathers," *Proceedings of the National Academy of Sciences of the United States of America*, vol. 100, no. 22, pp. 12576–12578, 2003.

[4] R. C. McPhedran, N. A. Nicorovici, D. R. McKenzie et al., "Structural colours through photonic crystals," *Physica B: Condensed Matter*, vol. 338, no. 1-4, pp. 182–185, 2003.

[5] K. Kumar, H. Duan, R. S. Hegde, S. C. W. Koh, J. N. Wei, and J. K. W. Yang, "Printing colour at the optical diffraction limit," *Nature Nanotechnology*, vol. 7, no. 9, pp. 557–561, 2012.

[6] J. Olson, A. Manjavacas, T. Basu et al., "High chromaticity aluminum plasmonic pixels for active liquid crystal displays," *ACS Nano*, vol. 10, no. 1, pp. 1108–1117, 2016.

[7] A. S. Roberts, A. Pors, O. Albrektsen, and S. I. Bozhevolnyi, "Subwavelength plasmonic color printing protected for ambient use," *Nano Letters*, vol. 14, no. 2, pp. 783–787, 2014.

[8] W. L. Barnes, A. Dereux, and T. W. Ebbesen, "Surface plasmon subwavelength optics," *Nature*, vol. 424, no. 6950, pp. 824–830, 2003.

[9] E. Laux, C. Genet, T. Skauli, and T. W. Ebbesen, "Plasmonic photon sorters for spectral and polarimetric imaging," *Nature Photonics*, vol. 2, no. 3, pp. 161–164, 2008.

[10] T. Xu, Y.-K. Wu, X. Luo, and L. J. Guo, "Plasmonic nanoresonators for high-resolution colour filtering and spectral imaging," *Nature Communications*, vol. 1, no. 1, p. 59, 2010.

[11] S. Yokogawa, S. P. Burgos, and H. A. Atwater, "Plasmonic color filters for CMOS image sensor applications," *Nano Letters*, vol. 12, no. 8, pp. 4349–4354, 2012.

[12] R. Rajasekharan, E. Balaur, A. Minovich et al., "Filling schemes at submicron scale: development of submicron sized plasmonic colour filters," *Scientific Reports*, vol. 4, no. 1, p. 6435, 2015.

[13] J. S. Clausen, E. Højlund-Nielsen, A. B. Christiansen et al., "Plasmonic metasurfaces for coloration of plastic consumer products," *Nano Letters*, vol. 14, no. 8, pp. 4499–4504, 2014.

[14] Y.-K. R. Wu, A. E. Hollowell, C. Zhang, and L. J. Guo, "Angle-insensitive structural colours based on metallic nanocavities and coloured pixels beyond the diffraction limit," *Scientific Reports*, vol. 3, no. 1, p. 1194, 2013.

[15] S. J. Tan, L. Zhang, D. Zhu et al., "Plasmonic color palettes for photorealistic printing with aluminum nanostructures," *Nano Letters*, vol. 14, no. 7, pp. 4023–4029, 2014.

[16] F. Lütolf, M. Stalder, and O. J. F. Martin, "Metallized gratings enable color effects and floating screen films by first-order diffraction," *Advanced Optical Materials*, vol. 3, no. 12, pp. 1793–1799, 2015.

[17] M. Rezaei, H. Jiang, and B. Kaminska, "Structural colour printing from a reusable generic nanosubstrate masked for the target image," *Nanotechnology*, vol. 27, no. 8, article 085301, 2016.

[18] Y. H. Fu, A. I. Kuznetsov, A. E. Miroshnichenko, Y. F. Yu, and B. Luk'yanchuk, "Directional visible light scattering by silicon nanoparticles," *Nature Communications*, vol. 4, no. 1, p. 1527, 2013.

[19] S. Person, M. Jain, Z. Lapin, J. J. Sáenz, G. Wicks, and L. Novotny, "Demonstration of zero optical backscattering from single nanoparticles," *Nano Letters*, vol. 13, no. 4, pp. 1806–1809, 2013.

[20] B. Rolly, B. Stout, and N. Bonod, "Boosting the directivity of optical antennas with magnetic and electric dipolar resonant particles," *Optics Express*, vol. 20, no. 18, pp. 20376–20386, 2012.

[21] A. E. Krasnok, A. E. Miroshnichenko, P. A. Belov, and Y. S. Kivshar, "All-dielectric optical nanoantennas," *Optics Express*, vol. 20, no. 18, article 20599, 20604 pages, 2012.

[22] I. Staude, A. E. Miroshnichenko, M. Decker et al., "Tailoring directional scattering through magnetic and electric resonances in subwavelength silicon nanodisks," *ACS Nano*, vol. 7, no. 9, pp. 7824–7832, 2013.

[23] M. L. Brongersma, Y. Cui, and S. Fan, "Light management for photovoltaics using high-index nanostructures," *Nature Materials*, vol. 13, no. 5, pp. 451–460, 2014.

[24] M. Decker and I. Staude, "Resonant dielectric nanostructures: a low-loss platform for functional nanophotonics," *Journal of Optics*, vol. 18, no. 10, article 103001, 2016.

[25] J. Proust, F. Bedu, B. Gallas, I. Ozerov, and N. Bonod, "All-dielectric colored metasurfaces with silicon Mie resonators," *ACS Nano*, vol. 10, no. 8, pp. 7761–7767, 2016.

[26] T. Wood, M. Naffouti, J. Berthelot et al., "All-dielectric color filters using SiGe-based Mie resonator arrays," *ACS Photonics*, vol. 4, no. 4, pp. 873–883, 2017.

[27] C.-S. Park, V. R. Shrestha, W. Yue et al., "Structural color filters enabled by a dielectric metasurface incorporating hydrogenated amorphous silicon nanodisks," *Scientific Reports*, vol. 7, no. 1, p. 2556, 2017.

[28] A. I. Kuznetsov, A. E. Miroshnichenko, M. L. Brongersma, Y. S. Kivshar, and B. Luk'yanchuk, "Optically resonant dielectric nanostructures," *Science*, vol. 354, no. 6314, article aag2472, 2016.

[29] S. Hong, Y. J. Lee, K. Moon, and S.-H. Kwon, "Double resonance perfect absorption in a dielectric nanoparticle array," *Current Optics and Photonics*, vol. 1, no. 3, pp. 228–232, 2017.

[30] N. A. Butakov and J. A. Schuller, "Designing multipolar resonances in dielectric metamaterials," *Scientific Reports*, vol. 6, no. 1, article 38487, 2016.

[31] U. Zywietz, A. B. Evlyukhin, C. Reinhardt, and B. N. Chichkov, "Laser printing of silicon nanoparticles with resonant optical electric and magnetic responses," *Nature Communications*, vol. 5, no. 1, p. 3402, 2014.

[32] J.-M. Y. Carrillo and A. V. Dobrynin, "Dynamics of nanoparticle adhesion," *The Journal of Chemical Physics*, vol. 137, no. 21, article 214902, 2012.